Enhanced Spin-Orbit Torque and Multilevel Current-Induced Switching in W/Co-Tb/Pt Heterostructure

Zhenyi Zheng,[1,2] Yue Zhang,[1,][*] Xueqiang Feng,[1] Kun Zhang,[1] Jiang Nan,[1] Zhizhong Zhang,[1,2] Guanda Wang,[1] Jinkai Wang,[1] Na Lei,[1] Dijun Liu,[2] Youguang Zhang,[1,2] and Weisheng Zhao[1,][†]

[1]*Fert Beijing Research Institute, BDBC, School of Microelectronics, Beihang University, 100191 Beijing, P. R. China*
[2]*School of Electronics and Information Engineering, Beihang University, 100191 Beijing, P. R. China*

Spin-orbit torque (SOT) driven magnetization switching in ferrimagnets (FIMs) can inspire a variety of low-power, high-speed, and multifunctional spintronic devices. SOT efficiency in ferrimagnet/heavy-metal (FIM/HM) systems has recently been found to be increased when the FIM is approaching its magnetic compensation point. However, the effective spin Hall angle cannot be obviously augmented due to the magnetization reduction. We investigate an enhanced SOT effect in a heterostructure composed of a near-compensated Co-Tb layer sandwiched by W and Pt layers, where Co-Tb is a rare-earth–transition-metal ferrimagnetic alloy with bulk perpendicular magnetic anisotropy and W has the opposite spin Hall angle to Pt. Beyond a large SOT efficiency, a 1.9 times more effective spin Hall angle and 20% switching power consumption can be achieved by optimizing the thickness of the HM layers compared to SOT-driven magnetization switching in a conventional FIM/HM structure. Moreover, based on this heterostructure, four-state current-induced magnetization switching is carried out. This work provides an alternative way to enhance the SOT effect in FIM/HM systems and promotes the use of FIMs for future high-performance memory and computation.

I. INTRODUCTION

Spin-orbit torque (SOT) has been widely considered to be an effective method to manipulate electron spins with low power dissipation and fast speed [1–4]. A large amount of work involving efficient current-induced magnetization switching [5–7] and domain wall (DW) motion driven by the SOT effect [8–11] in ferromagnet/heavy-metal (FM/HM) structures has been implemented, which offers great perspective for memory and logic devices [12–16]. Recently, ferrimagnets (FIMs) have drawn wide attention because: (1) they can exhibit ultrafast dynamics like antiferromagnets (AFMs), which shortens the magnetization switching time from a nanosecond order, which normally occurs in FMs, to a picosecond order [17,18]; (2) they can avoid magnetic field immunity, which overcomes the detection difficulties of AFMs for practical applications [19,20]; and (3) some of them can provide bulk perpendicular magnetic anisotropy (PMA), which solves the insufficient thermal stability issue caused by the downscaling of FMs with interfacial PMA [21,22]. Hence, investigations on the magnetic behavior of FIMs under the SOT effect are of significance to develop high-performance spintronic devices.

Rare-earth–transition-metal (RE-TM) alloys (e.g., Co-Tb, Co-Fe-Gd, etc.) are classic ferrimagnetic material systems in which the RE and TM sublattices are antiferromagnetically coupled to each other. By changing the chemical composition or temperature, the magnetization and angular momentum of alloys can be precisely and significantly tuned [18,19,23–31]. Based on this mechanism, RE-TM alloys exhibit abundant and fascinating characteristics near their magnetic compensation point (MCP) and angular momentum compensation point (AMCP). The MCP appears when the magnetizations of two sublattices totally compensate each other. The AMCP is mainly related to the magnetic dynamic behaviors. When coming to this point, ultrafast magnetization switching and DW motion have been observed [19,23,24]. Previous literature demonstrated that the current-induced SOT efficiency [$\chi = (H_{\mathrm{eff}}/J_e)$, where H_{eff} is the effective field and J_e is the injected current density] can be significantly improved in near-compensated FIM/HM bilayer systems [27–31]. However, the effective spin Hall angle $\theta_{\mathrm{SH}}^{\mathrm{eff}}$ cannot be obviously augmented due to the magnetization reduction near

―――――――
[*]yz@buaa.edu.cn
[†]weisheng.zhao@buaa.edu.cn

044032-1

the MCP, since

$$\theta_{\text{SH}}^{\text{eff}} = \frac{2e}{\hbar} \frac{M_s t_{\text{FIM}} H_{\text{eff}}}{J_e}, \qquad (1)$$

where M_s and t_{FIM} are the net magnetization and thickness of the FIM [27–30]. Meanwhile, compared with a FM/HM system, $\theta_{\text{SH}}^{\text{eff}}$ is compressed in a HM-FIM system due to a relatively small spin mixing conductance at the interface [27,30,32]. These realities directly degrade the SOT effect on FIM-based devices and hinder their future low-power application.

In this work, a $W/Co_xTb_{1-x}/Pt$ heterostructure is investigated to offer an enhanced SOT effect. First, by varying the element concentrations of Co and Tb, the MCP of Co_xTb_{1-x} is experimentally determined at room temperature. We then carry out SOT-driven magnetization switching of Co-Tb near the MCP with varied thicknesses of a capping Pt layer. Beyond a large SOT efficiency, a 1.9 times effective spin Hall angle and 20% switching power consumption compared with the conventional W/Co-Tb structure can be achieved, which is due to the opposite spin Hall angles of W and Pt as well as the optimized average resistivity. Finally, based on the W/Co-Tb/Pt heterostructure, a multilayer consisting of two Co-Tb layers is fabricated and four-state current-induced magnetization switching is realized. This SOT enhancement approach and multilevel switching can be beneficial to the application of ferrimagnetic material systems in future memory and logic devices.

II. MCP DETERMINATION OF FERRIMAGENTIC ALLOY AND LARGE SOT EFFICIENCY NEAR MCP

As shown in Fig. 1(a), we deposit a series of $W(5)/Co_xTb_{1-x}(4)/Pt(t_{Pt})$ (thickness in nm) stacks on thermally oxidized silicon substrates by dc and rf magnetic sputtering under a base pressure lower than 3×10^{-8} Torr. The alloy Co_xTb_{1-x} is grown by the cosputtering of Co and Tb targets. Various Co concentrations x (in a range from 0.61 to 0.83) are achieved by tuning the sputtering power of the Co target. First, the magnetic compensation point of the ferrimagnetic Co_xTb_{1-x} alloy is studied by fixing the thickness of Pt to 2 nm. Vibration sample magnetometry (VSM) is utilized to determine the coercive field and net magnetization of each sample [see Fig. 1(b)]. The dependence of net magnetization M_s (black squares) on Co concentrations follows a certain trend line (red dash line, detailed calculation in Ref. [43]), and M_s tends to vanish when x is crossing 0.705. In addition, a divergent coercive field (blue circles) occurs as well near this concentration. Thus, the MCP can be determined as 0.705. In addition, anomalous Hall effect (AHE) measurement results [see inset of Fig. 1(b)] reveal the good PMA properties of our
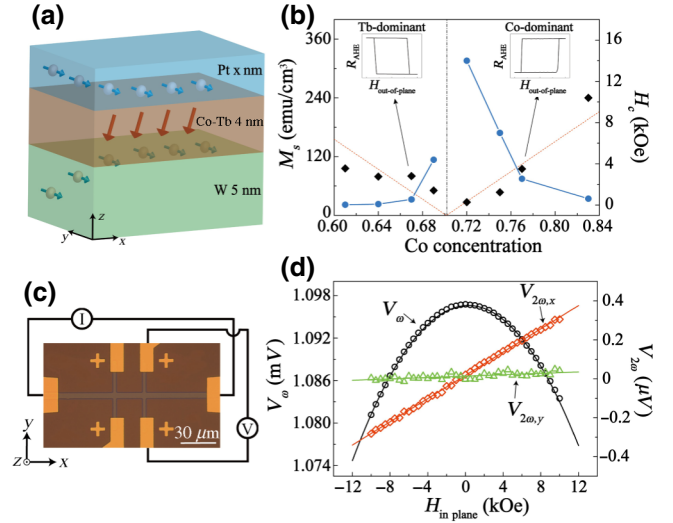

FIG. 1.   (a) Schematic of deposited W/Co-Tb/Pt samples. (b) Coercivities (blue circles) and net magnetizations (black squares) of deposited films with different Co concentrations. The right part corresponds to the Co-dominant area and the left corresponds to the Tb-dominant area. The two inserts reveal opposite AHE signs crossing the MCP. (c) Image of 5-μm-width Hall bar device with harmonics measurement setup. (d) Harmonics measurement data for near-compensated $Co_{0.72}Tb_{0.28}$ sample. Dampinglike signals (red line) show good linearity in a small magnetic field range and is much larger than the fieldlike signals (green line).

samples. The sign change of AHE when Co concentration is crossing the MCP confirms that the transport properties of deposited RE-TM alloys are dominated by the $3d$ orbitals of TM elements near the Fermi level [24–31].

Harmonics measurement is then implemented on a fabricated 5-μm-width Hall bar with near-compensated $Co_{0.72}Tb_{0.28}$ [schematics in Fig. 1(c)], by injecting an ac current of 133.33 Hz along the x axis. Two SR830 lock-in amplifiers are used to detect the harmonic signals. Figure 1(d) plots the curves of the first- and second-harmonic voltages, that is, V_ω and $V_{2\omega,x(y)}$, versus the in-plane magnetic field. The respective curvature of V_ω and the slope of $V_{2\omega,x(y)}$ could be used to calculate a ratio coefficient $B_{x(y)}$ [33,34],

$$B_{x(y)} = \left(\frac{\partial V_{2\omega}}{\partial H_{x(y)}} \right) \left(\frac{\partial^2 V_\omega}{\partial H_{x(y)}^2} \right)^{-1}. \qquad (2)$$

Then, the dampinglike H_{dl} and fieldlike effective field H_{fl} can be determined by the following relation [33,34]:

$$H_{\text{dl(fl)}} = -2 \frac{B_{x(y)} \pm 2\xi B_{y(x)}}{1 - 4\xi^2}, \qquad (3)$$

where ξ is the ratio of the planar Hall resistance R_{PHE} and AHE resistance R_{AHE}. It is worthwhile to note that the

measured R_{PHE} in our samples is much smaller than R_{AHE}, which yields a tiny ξ [43]. Thus, $H_{dl(fl)} \approx -2B_{x(y)}$. We also find that the slope of $V_{2\omega,x}$ induced by the field along the x axis is much larger than the slope of $V_{2\omega,y}$ induced by the field along the y axis, which indicates that H_{fl} is negligible compared to H_{dl}. Therefore, only the dampinglike SOT effect is discussed in our work.

To determine the effective current density in heavy metals W and Pt, the resistivities of W (151 $\mu\Omega$ cm), Co-Tb, (295 $\mu\Omega$ cm), and Pt (27 $\mu\Omega$ cm) are measured by four-point measurements. Considering the fact that both Pt and W heavy-metal layers are involved to induce the SOT effect, the average current density $J_{HM,avg}$ is introduced in the calculation of SOT efficiency χ [43]. The Joule heating effect is eliminated since the calculated effective damping-like field varies linearly with the increasing injected current. The determined χ in the W(5)/Co$_{0.72}$Tb$_{0.28}$(4)/Pt(2) sample is 59 ± 4 (10^{-10} Oe m^2/A), which is 1.6 times 37 (10^{-10} Oe m^2/A) as reported in near-compensated W/Co-Tb/Al systems [28], 4.9 times 12 (10^{-10} Oe m^2/A) reported in near-compensated Ta/Co-Tb/Ru systems [27], and more than 5 times 9–10 (10^{-10} Oe m^2/A) reported in conventional β-W/Co-Fe-B/MgO systems [35,36]. This large χ could be mainly explained by the divergent SOT efficiency tendency near the MCP. Meanwhile, the enhanced SOT effect by the coeffect of W and Pt also contributes to the augmentation of χ, which will be analyzed in detail in Sec. III.

III. THICKNESS-DEPENDENT SOT ENHANCEMENT IN NEAR-COMPENSATED W/Co$_{0.72}$Tb$_{0.28}$/Pt HETEROSTRUCTURE

Previous work has demonstrated that capping a HM with opposite spin Hall angle on a Pt/FM bilayer could induce an enhanced SOT [37,38]. Nevertheless, the coeffect of opposite spin Hall angles has not been elucidated clearly, because Ta or W, whose spin Hall angles are already larger than Pt, have been used as the capping layer. In order to better distinguish the origin of the enhancement, we cap Pt on a W(5)/Co$_{0.72}$Tb$_{0.28}$(4) bilayer and vary the thickness of Pt, that is t_{Pt}, from 2 to 5 nm. A control sample (reference) W(5)/Co$_{0.72}$Tb$_{0.28}$(4)/AlO$_x$(1)/Ta(2), in which t_{Pt} is considered as zero, is also fabricated to demonstrate the influence of Pt.

We first verify the compensated property of all the samples with different HM layer thicknesses. As shown in Fig. 2(a), each sample exhibits a negligible value of M_s (<40 emu/cm^3) compared to that of the Co$_{0.83}$Tb$_{0.17}$ sample, which is far from the MCP and those of typical ferromagnetic material systems with PMA [see inset of Fig. 2(a)]. It further reveals that our samples are near compensated. Figure 2(b) demonstrates the magnetization switching curves of the samples induced by a 0.1-ms-width pulse current. In order to complete the switching process,
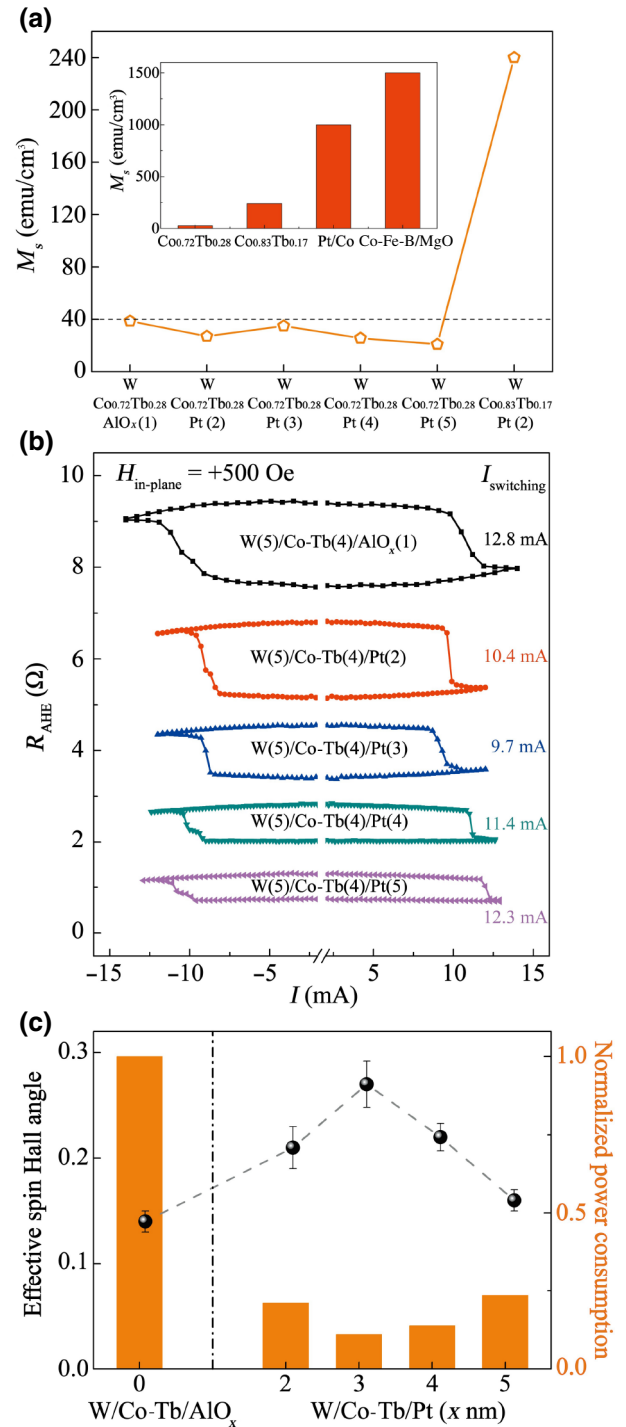

FIG. 2. (a) Dependence of net magnetization of near-compensated Pt/Co$_{0.72}$Tb$_{0.28}$/W samples versus t_{Pt}. The inset shows the net magnetization comparison among different material systems to demonstrate the near-compensated property of our samples. (b) Current-induced SOT switching curves of W(5)/Co$_{0.72}$Tb$_{0.28}$/Pt(t_{Pt}) samples under an in-plane magnetic field $H_{in\ plane}$ = 500 Oe, where t_{Pt} varies from 2 to 5 nm. (c) Dependence of effective spin Hall angle (black circles) and normalized power consumption (orange bars) for switching the Co-Tb layer versus thickness of the Pt layer. An optimal point occurs at 3-nm-thick Pt.

an in-plane field as large as $+500$ Oe is applied along the injected current direction to break the dynamic symmetry. With the increase of t_{Pt}, the AHE resistance decreases since less current passes through the magnetic layer. Meanwhile, the switching current threshold first decreases and then increases, despite the consistently increasing total thickness of HM. Hence, a variation of the SOT effect is also expected in the different samples.

Based on the harmonics measurements and Eq. (1), the considerable enhancement of the SOT effect is illustrated in Fig. 2(c) via the value of the effective dampinglike spin Hall angle θ_{SH}^{eff}. θ_{SH}^{eff} augments from 0.21 ± 0.02 to 0.27 ± 0.02 when t_{Pt} varies from 2 to 3 nm. We notice that both of these values are much larger than that of the reference sample W/Co$_{0.72}$Tb$_{0.28}$/AlO$_x$ ($\theta_{SH}^{eff} \approx 0.14 \pm 0.01$), which verifies that the SOT enhancement is due to the capping Pt. However, when t_{Pt} exceeds 3 nm, θ_{SH}^{eff} starts to diminish. To explain this phenomenon, a model of θ_{SH}^{eff} vs t_{Pt} is built:

$$\theta_{SH}^{eff}(t_{Pt}) = \theta_{W}^{eff}\left[1 - \frac{\rho_W - \rho_{Pt}}{\rho_W + \rho_{Pt}t_W\frac{1}{t_{Pt}}}\right]$$
$$+ \theta_{Pt}^{eff}\left[1 + \frac{\rho_W - \rho_{Pt}}{\rho_{Pt} + \frac{\rho_W}{t_W}t_{Pt}}\right], \quad (4)$$

where θ_{Pt}^{eff} and θ_{W}^{eff} are the effective spin Hall angles of Pt and W, ρ_W and ρ_{Pt} are the resistivities of W and Pt, and t_W is the thickness of W. According to the model, this behavior can be explained in two aspects: (1) The SOT effect of Pt mainly comes from the bulk spin Hall effect (SHE). In this case, the effective spin Hall angle coming from Pt, that is, θ_{Pt}^{eff}, is a thickness-dependent value and can be described by the diffusion model [4,36]

$$\theta_{Pt}^{eff}(t_{Pt}) = \theta_{Pt}^{eff}(t_{Pt} \to \infty)\left[1 - \text{sech}\left(\frac{t_{Pt}}{\lambda_{SF}}\right)\right], \quad (5)$$

where $\theta_{Pt}^{eff}(t_{Pt} \to \infty)$ and λ_{SF} are the thickness-saturated effective spin Hall angle and the spin diffusion length of Pt, respectively. The λ_{SF} of Pt was previously reported as approximately 3 nm [4]; hence, the increment of $\theta_{SH,Pt}^{eff}$ will slow down considerably when $t_{Pt} > \lambda_{SF}$. (2) The former part of Eq. (4) indicates that a thicker Pt layer will shunt a larger part of the injected current, which causes less current passing through the W layer. Therefore, the enhancement effect is weakened when the thickness of the Pt layer reaches a relatively large value.

Furthermore, power consumption for the SOT-induced magnetization switching of the Co-Tb ferrimagnetic layer is analyzed, as it evaluates the SOT effect from another angle and is of great significance toward a realistic application. Power consumption is proportional to j_{sw}^2/σ_{HM}, where j_{sw} and σ_{HM} represent the critical switching current density

and the conductance of heavy metal [39]. As the critical switching current density is inversely proportional to the spin Hall angle θ_{SH}^{eff}, $\rho_{HM, avg} \times \theta_{SH}^{eff-2}$ is used for estimating the power consumption [40], where $\rho_{HM, avg}$ is the average resistivity of heavy metals (W and Pt). Through electrical transport properties' measurements, we notice that the capping Pt with low resistivity could efficiently reduce the device resistance, while the width and length of the Hall bars remain constant. $\rho_{HM,avg}$ is then calculated, and it has a similar decreasing tendency with the device resistance when t_{Pt} continues to increase [43]. As shown by the orange bars in Fig. 2(c), capping a Pt layer on a W/Co-Tb bilayer helps to effectively reduce the power consumption, which is due to the enhanced θ_{SH}^{eff} as well as the lowered average resistivity in HMs. Corresponding to the spin Hall angle, the power consumption reaches its minimum when t_{Pt} is equal to 3 nm. If t_{Pt} keeps increasing, this value will rise and finally approach a saturation that can be regarded as the case with a single Pt layer. In addition, the added Pt layer also hinders the current shunting in the magnetic layer, which also contributes to the power consumption reduction.

IV. FOUR MAGNETIC STATES SWITCHING IN Pt/Co-Tb/W/Co-Tb/Pt HETEROSTRUCTURE

It should be noticed that both of sides of the HM layer would accumulate electron spins (but in opposite directions) after a current is applied, however, only the effect of one side is usually considered in normal SOT devices. The aforementioned enhanced SOT effect due to two HMs with opposite spin Hall angles provides an alternative to leverage both of sides of the HMs to realize efficient and multilevel magnetization switching. Here, a heterostructure with two near-compensated Co-Tb layers, Pt(3)/Co$_{0.72}$Tb$_{0.28}$(2)/W(5)/Co$_{0.72}$Tb$_{0.28}$(4)/Pt(3), is deposited as illustrated in Fig. 3(a). Figure 3(b) shows a transmission electron microscope (TEM) image of the cross section of this multilayer. The intermediate 5-nm-thick W layer is thick enough to avoid the coupling effect between two ferrimagnetic Co-Tb layers, which is proven by the AHE measurement of 5-μm-width Hall bars in Fig. 3(c). The R_{AHE} change at the smaller coercive field (approximately 0.11 T) corresponds to the switching of the thinner Co-Tb layer (2-nm-thick), while the R_{AHE} changes at the larger coercive field (approximately 1 T) corresponds to the switching of the thicker Co-Tb layer (4-nm-thick). Note that this difference of coercive fields is mainly caused by the varied volume anisotropy energy barrier due to the change of thickness, rather than the change of element concentration.

Four-state SOT-induced magnetization switching is carried out by sweeping a 0.1-ms-pulse current from 16 to -16 mA under a 50 Oe in-plane magnetic field along the current direction (x axis). As shown in Fig. 4(a),
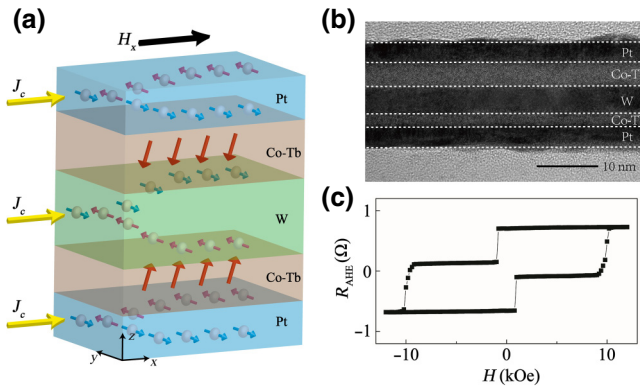
FIG. 3. (a) Schematic of the $Pt(3)/Co_{0.72}Tb_{0.28}(2)/W(5)/Co_{0.72}Tb_{0.28}(4)/Pt(3)$ heterostructure and SOT effect induced by applied current in the system. (b) TEM image of the cross section of the deposited multilayer. (c) AHE measurement curve of fabricated Hall bars. The two stable intermediate states confirm that no coupling effect between two Co-Tb layers occurs in the system.

the initial magnetization state of two ferrimagnetic layers is $(Co-Tb_{thin,\uparrow}, Co-Tb_{thick,\downarrow})$. When the current sweeps to -7 mA, a decrease of 0.4 Ω in R_{AHE} occurs. In this case, the thinner Co-Tb layer can be switched to the "down" state, and a $(Co-Tb_{thin,\downarrow}, Co-Tb_{thick,\downarrow})$ state is thus achieved. If current sweeps to -13 mA, the thicker Co-Tb layer can also be switched to "up" state, which leads to an increase of 0.6 Ω in R_{AHE} with a $(Co-Tb_{thin,\downarrow}, Co-Tb_{thick,\uparrow})$ state. Correspondingly, when the current sweeps back from -16 to 16 mA, states of $(Co-Tb_{thin,\uparrow}, Co-Tb_{thick,\uparrow})$ and $(Co-Tb_{thin,\uparrow}, Co-Tb_{thick,\downarrow})$ can be achieved in sequence at 7 and 13 mA. Similar switching behaviors are also observed at larger applied in-plane fields (±500, ±200 Oe). The switching current threshold of each layer scales down when the in-plane magnetic field increases, which obeys the Landau-Lifshitz-Gilbert (LLG) equations [41]. We also notice that there exist some intermediate anomalous Hall resistance states, especially in the samples with large in-plane fields. This can be possibly explained by multidomain states induced by the inhomogeneity of Co-Tb films during the magnetization switching process.

Individual control of the magnetizations of two Co-Tb layers is also achieved once a single 0.1-ms pulse is applied with a magnitude of 10 or 15 mA under a 50-Oe magnetic field along x axis. After each pulse operation, a dc current of 0.1 mA is injected into the device to detect the magnetization states of two Co-Tb layers by AHE voltage. This measurement is implemented 10 times to evaluate the stability of each state. As shown in Fig. 4(b), when two pulses of -15 and $+10$ mA are successively injected into device, a stable $(Co-Tb_{thin,\uparrow}, Co-Tb_{thick,\uparrow})$ state is achieved. Similarly, a $(Co-Tb_{thin,\downarrow}, Co-Tb_{thick,\downarrow})$ state could be obtained if two pulses of $+15$ and -10 mA are applied in
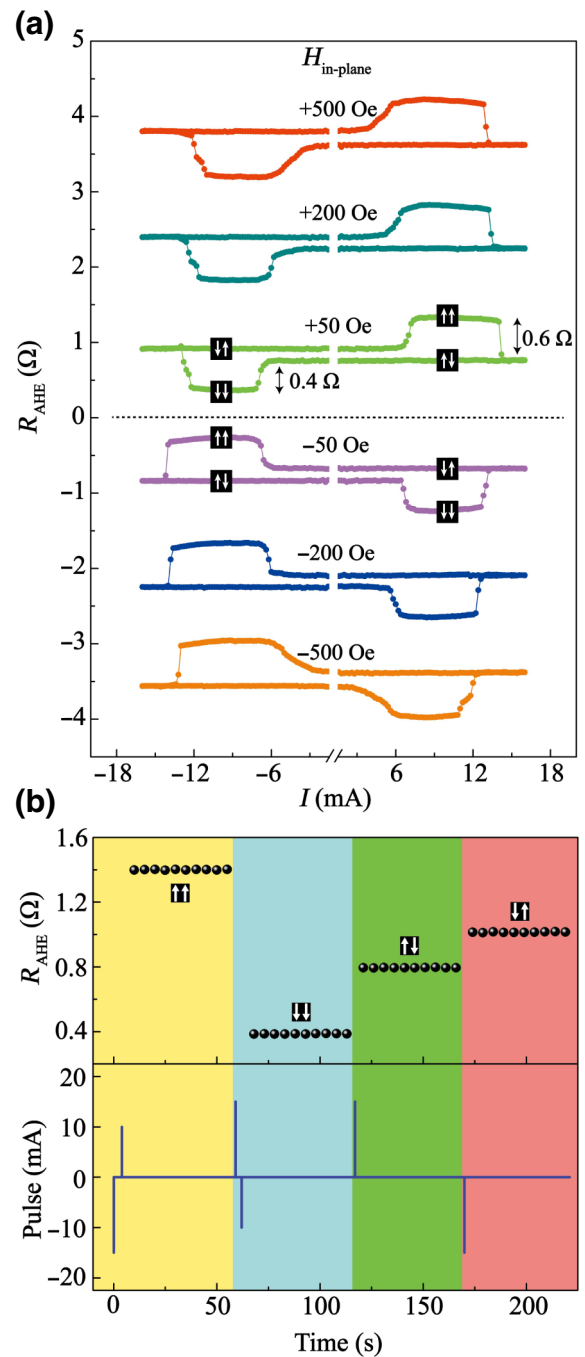

FIG. 4. (a) Multilevel current-induced switching of near-compensated Pt/Co-Tb/W/Co-Tb/Pt heterostructure under different in-plane magnetic fields. (b) Stable four states controlled by a sequence of pulses and a 50-Oe in-plane magnetic field.

sequence. Moreover, injecting single $+15$ or -15 mA pulses are capable of writing $(Co-Tb_{thin,\uparrow}, Co-Tb_{thick,\downarrow})$ and $(Co-Tb_{thin,\downarrow}, Co-Tb_{thick,\uparrow})$ states, respectively. If we assume that $(Co-Tb_{thin,\downarrow}, Co-Tb_{thick,\downarrow})$, $(Co-Tb_{thin,\downarrow}, Co-Tb_{thick,\uparrow})$, $(Co-Tb_{thin,\uparrow}, Co-Tb_{thick,\downarrow})$, and $(Co-Tb_{thin,\uparrow},$

Co-Tb$_{thick,\uparrow}$) could represent data groups (0,0), (0,1), (1,0), and (1,1), respectively, the capacity of a single SOT device could be doubled.

In addition, the working current density of this heterostructure again confirms the high SOT effect in a W/Co-Tb/Pt structure. Near-compensated Co-Tb with a total thickness of 6 nm could be switched under a current density of 1.95×10^{11} A/m^2 and a 50 Oe in-plane magnetic field. For comparison, in a similar Pt/Co/Pt/Co/Pt system, a more than or equal to 1000 Oe in-plane field and a 2.9×10^{11} A/m^2 current density are required to switch a 1.1-nm Co layer [42]; in a W/Co-Tb/Al system, a 1000 Oe in-plane field and 4.5×10^{11} A/m^2 current density are required to switch a 3.5-nm near-compensated Co-Tb layer [28].

V. CONCLUSION

In summary, we propose and characterize a system composed of a near-compensated ferrimagnetic alloy sandwiched by two HM layers with opposite spin Hall angles that provides not only high SOT efficiency but also an enhanced effective spin Hall angle. The coeffect of two HMs is investigated through adjusting the thickness of the capping Pt layer in a series of W/Co-Tb/Pt samples. By taking material resistivity into consideration, an optimal point (3 nm in our work) is found to provide the most prominent improvement in terms of effective spin Hall angle and power consumption. Based on this enhancement mechanism, multilevel magnetization switching is realized in a Pt/Co-Tb/W/Co-Tb/Pt multilayer, which not only doubles the storage capacity, but also requires a much smaller magnetic field than FM/HM systems. Our work combining efficient and multibit magnetization switching provides an alternative route to leverage ferrimagnetic material in future spintronic devices.

ACKNOWLEDGMENTS

Z.Z. and Y.Z. contributed equally to this work.

[1] J. E. Hirsch, Spin Hall Effect, Phys. Rev. Lett. **83**, 1834 (1999).

[2] L. Liu, C. F. Pai, Y. Li, H. W. Tseng, D. C. Ralph, and R. A. Buhrman, Spin-torque switching with the giant spin Hall effect of tantalum, Science **336**, 555 (2012).

[3] I. M. Miron, G. Gaudin, S. Auffret, B. Rodmacq, A. Schuhl, S. Pizzini, J. Vogel, and P. Gambardella, Current-driven spin torque induced by the Rashba effect in a ferromagnetic metal layer, Nat. Mater. **9**, 230 (2010).

[4] L. Liu, T. Moriyama, D. C. Ralph, and R. A. Buhrman, Spin-Torque Ferromagnetic Resonance Induced by the Spin Hall Effect, Phys. Rev. Lett. **106**, 036601 (2011).

[5] Y. C. Lau, D. Betto, K. Rode, J. M. D. Coey, and P. Stamenov, Spin–orbit torque switching without an external field using interlayer exchange coupling, Nat. Nanotechnol. **11**, 758 (2016).

[6] G. Yu, P. Upadhyaya, Y. Fan, J. G. Alzate, W. Jiang, K. L. Wong, S. Takei, S. Bender, L. Chang, Y. Jiang, M. Lang, J. Tang, Y. Wang, Y. Tserkovnyak, P. K. Amiri, and K. L. Wang, Switching of perpendicular magnetization by spin–orbit torques in the absence of external magnetic fields, Nat. Nanotechnol. **9**, 548 (2014).

[7] M. Wang, W. Cai, D. Zhu, Z. Wang, J. Kan, Z. Zhao, K. Cao, Z. Wang, Y. Zhang, T. Zhang, C. Park, J. P. Wang, A. Fert, and W. Zhao, Field-free switching of a perpendicular magnetic tunnel junction through the interplay of spin–orbit and spin-transfer torques, Nat. Electron. **1**, 582 (2018).

[8] S. Emori, U. Bauer, S. M. Ahn, E. Martinez, and G. S. Beach, Current-driven dynamics of chiral ferromagnetic domain walls, Nat. Mater. **12**, 611 (2013).

[9] K. S. Ryu, L. Thomas, S. H. Yang, and S. Parkin, Chiral spin torque at magnetic domain walls, Nat. Nanotechnol. **8**, 527 (2013).

[10] Y. Zhang, W. Zhao, J. O. Klein, C. Chappert, and D. Ravelosona, Peristaltic perpendicular-magnetic-anisotropy racetrack memory based on chiral domain wall motions, J. Phys. D-Appl. Phys. **48**, 105001 (2015).

[11] J. Torrejon, J. Kim, J. Sinha, S. Mitani, M. Hayashi, M. Yamanouchi, and H. Ohno, Interface control of the magnetic chirality in CoFeB/MgO heterostructures with heavy-metal underlayers, Nat. Commun. **5**, 4655 (2014).

[12] C. Wan, X. Zhang, Z. Yuan, C. Fang, W. Kong, Q. Zhang, H. Wu, U. Khan, and X. Han, Programmable spin logic based on spin Hall effect in a single device, Adv. Electron. Mater. **3**, 1600282 (2017).

[13] K. Zhang, Y. Zhang, Z. Zhang, Z. Zheng, G. Wang, Y. Zhang, Q. Liu, S. Yan, and W. Zhao, Large magnetoresistance and 15 boolean logic functions based on a ZnCoO film and diode combined device, Adv. Electron. Mater. **5**, 1800812 (2019).

[14] D. Bhowmik, L. You, and S. Salahuddin, Spin Hall effect clocking of nanomagnetic logic without a magnetic field, Nat. Nanotechnol. **9**, 59 (2014).

[15] S. Luo, M. Song, X. Li, Y. Zhang, J. Hong, X. Yang, X. Zhou, N. Xu, and L. You, Reconfigurable skyrmion logic gates, Nano Lett. **18**, 1180 (2018).

[16] G. Wang, Y. Zhang, B. Zhang, B. Wu, J. Nan, X. Zhang, Z. Zhang, J. Klein, D. Ravelosona, Z. Wang, Y. Zhang, and

W. Zhao, Ultra-dense ring-shaped racetrack memory cache design, IEEE Trans. Circ. Syst. I Reg. Pap. **66**, 215 (2019).

[17] J. C. Sankey, P. M. Braganca, A. G. F. Garcia, I. N. Krivorotov, R. A. Buhrman, and D. C. Ralph, Spin-Transfer-Driven Ferromagnetic Resonance of Individual Nanomagnets, Phys. Rev. Lett. **96**, 227601 (2006).

[18] V. López-Flores, N. Bergeard, V. Halté, C. Stamm, N. Pontius, M. Hehn, E. Otero, E. Beaurepaire, and C. Boeglin, Role of critical spin fluctuations in ultrafast demagnetization of transition-metal rare-earth alloys, Phys. Rev. B **87**, 214412 (2013).

[19] K. J. Kim, S. K. Kim, Y. Hirata, S. H. Oh, T. Tono, D. H. Kim, T. Okuno, W. S. Ham, S. Kim, G. Go, Y. Tserkovnyak, A. Tsukamoto, T. Moriyama, K. J. Lee, and T. Ono, Fast domain wall motion in the vicinity of the angular momentum compensation temperature of ferrimagnets, Nat. Mater. **16**, 1187 (2017).

[20] T. Jungwirth, X. Marti, P. Wadley, and J. Wunderlich, Antiferromagnetic spintronics, Nat. Nanotechnol. **11**, 231 (2016).

[21] N. Nishimura, T. Hirai, A. Koganei, T. Ikeda, K. Okano, Y. Sekiguchi, and Y. Osada, Magnetic tunnel junction device with perpendicular magnetization films for high-density magnetic random access memory, J. Appl. Phys. **91**, 5246 (2002).

[22] H. Wang, M. T. Rahman, H. Zhao, Y. Isowaki, Y. Kamata, A. Kikitsu, and J. P. Wang, Fabrication of FePt type exchange coupled composite bit patterned media by block copolymer lithography, J. Appl. Phys. **109**, 07B754 (2011).

[23] L. Caretta, M. Mann, F. Büttner, K. Ueda, B. Pfau, C. M. Günther, P. Hessing, A. Churikova, C. Klose, M. Schneider, D. Engel, C. Marcus, D. Bono, K. Bagschik, S. Eisebitt, and G. S. D. Beach, Fast current-driven domain walls and small skyrmions in a compensated ferrimagnet, Nat. Nanotechnol. **13**, 1154 (2018).

[24] S. A. Siddiqui, J. Han, J. T. Finley, C. A. Ross, and L. Liu, Current-Induced Domain Wall Motion in a Compensated Ferrimagnet, Phys. Rev. Lett. **121**, 057701 (2018).

[25] Z. Zhao, M. Jamali, A. K. Smith, and J. P. Wang, Spin Hall switching of the magnetization in Ta/TbFeCo structures with bulk perpendicular anisotropy, Appl. Phys. Lett. **106**, 132404 (2015).

[26] T. H. Pham, S. G. Je, P. Vallobra, T. Fache, D. Lacour, G. Malinowski, M. C. Cyrille, G. Gaudin, O. Boulle, M. Hehn, J. C. Rojas-Sánchez, and S. Mangin, Thermal Contribution to the Spin-Orbit Torque in Metallic-Ferrimagnetic Systems, Phys. Rev. Appl. **9**, 064032 (2018).

[27] J. Finley and L. Liu, Spin-Orbit-Torque Efficiency in Compensated Ferrimagnetic Cobalt-Terbium Alloys, Phys. Rev. Appl. **6**, 054001 (2016).

[28] S. G. Je, J. C. Rojas-Sánchez, T. H. Pham, P. Vallobra, G. Malinowski, D. Lacour, T. Fache, M. C. Cyrille, D. Y. Kim, S. B. Choe, M. Belmeguenai, M. Hehn, S. Mangin, G. Gaudin, and O. Boulle, Spin-orbit torque-induced switching in ferrimagnetic alloys: Experiments and modeling, Appl. Phys. Lett. **112**, 062401 (2018).

[29] K. Ueda, M. Mann, P. W. de Brouwer, D. Bono, and G. S. Beach, Temperature dependence of spin-orbit torques

across the magnetic compensation point in a ferrimagnetic TbCo alloy film, Phys. Rev. B **96**, 064410 (2017).

[30] W. Seung Ham, S. Kim, D. H. Kim, K. J. Kim, T. Okuno, H. Yoshikawa, A. Tsukamoto, T. Moriyama, and T. Ono, Temperature dependence of spin-orbit effective fields in Pt/GdFeCo bilayers, Appl. Phys. Lett. **110**, 242405 (2017).

[31] R. Mishra, J. Yu, X. Qiu, M. Motapothula, T. Venkatesan, and H. Yang, Anomalous Current-Induced Spin Torques in Ferrimagnets Near Compensation, Phys. Rev. Lett. **118**, 167201 (2017).

[32] T. C. Wang, T. Y. Chen, C. T. Wu, H. W. Yen, and C. F. Pai, Comparative study on spin-orbit torque efficiencies from W/ferromagnetic and W/ferrimagnetic heterostructures, Phys. Rev. Mater. **2**, 014403 (2018).

[33] M. Hayashi, J. Kim, M. Yamanouchi, and H. Ohno, Quantitative characterization of the spin-orbit torque using harmonic Hall voltage measurements, Phys. Rev. B **89**, 144425 (2014).

[34] K. Garello, I. M. Miron, C. O. Avci, F. Freimuth, Y. Mokrousov, S. Blügel, S. Auffret, O. Boulle, G. Gaudin, and P. Gambardella, Symmetry and magnitude of spin–orbit torques in ferromagnetic heterostructures, Nat. Nanotechnol. **8**, 587 (2013).

[35] C. F. Pai, L. Liu, Y. Li, H. W. Tseng, D. C. Ralph, and R. A. Buhrman, Spin transfer torque devices utilizing the giant spin Hall effect of tungsten, Appl. Phys. Lett. **101**, 122404 (2012).

[36] Q. Hao and G. Xiao, Giant Spin Hall Effect and Switching Induced by Spin-Transfer Torque in a $W/Co_{40}Fe_{40}B_{20}/MgO$ Structure With Perpendicular Magnetic Anisotropy, Phys. Rev. Appl. **3**, 034009 (2015).

[37] S. Woo, M. Mann, A. J. Tan, L. Caretta, and G. S. D. Beach, Enhanced spin-orbit torques in Pt/Co/Ta heterostructures, Appl. Phys. Lett. **105**, 212404 (2014).

[38] J. Yu, X. Qiu, W. Legrand, and H. Yang, Large spin-orbit torques in Pt/Co-Ni/W heterostructures, Appl. Phys. Lett. **109**, 042403 (2016).

[39] D. C. Mahendra, R. Grassi, J. Y. Chen, M. Jamali, D. R. Hickey, D. Zhang, Z. Zhao, H. Li, P. Quarterman, Y. Lv, M. Li, A. Manchon, K. A. Mkhoyan, T. Low, and J. P. Wang, Room-temperature high spin–orbit torque due to quantum confinement in sputtered $Bi_xSe_{(1-x)}$ films, Nat. Mater. **17**, 800 (2018).

[40] J. Han, A. Richardella, S. A. Siddiqui, J. Finley, N. Samarth, and L. Liu, Room-Temperature Spin-Orbit Torque Switching Induced by a Topological Insulator, Phys. Rev. Lett. **119**, 077702 (2017).

[41] S. Zhang and S. S. L. Zhang, Generalization of the Landau-Lifshitz-Gilbert Equation for Conducting Ferromagnets, Phys. Rev. Lett. **102**, 086601 (2009).

[42] Y. Sheng, Y. C. Li, X. Q. Ma, and K. Y. Wang, Current-induced four-state magnetization switching by spin-orbit torques in perpendicular ferromagnetic trilayers, Appl. Phys. Lett. **113**, 112406 (2018).

[43] See Supplemental Material at http://link.aps.org/supplemental/10.1103/PhysRevApplied.12.044032 for more details about magnetic compensation point determination, SOT efficiency calculation, and SOT enhancement phenomena near MCP.